metals

MDPI

Review

De-Ironing of Aluminium Alloy Melts by High Shear Melt Conditioning Technology: An Overview

Jaime Lazaro-Nebreda [1,*], Jayesh B. Patel [1], Kawther Al-Helal [1], Feng Gao [1], Ian Stone [1], Isaac T. H. Chang [1], Geoff M. Scamans [1,2] and Zhongyun Fan [1]

[1] Brunel Centre for Advanced Solidification Technology, Brunel University London, Uxbridge UB8 3PH, UK
[2] Innoval Technology Limited, Beaumont Cl, Banbury OX16 1TQ, UK
* Correspondence: jaime.lazaronebreda@brunel.ac.uk

Abstract: The main problem of recycling aluminium scrap is the gradual accumulation of impurities, especially iron, which tend to form undesired intermetallic compounds that affect the integrity and the mechanical performance of the castings. In this paper, we aim to provide an overview on the topic of iron removal from aluminium melts through primary intermetallic precipitation and the progress made during the LiME Hub project to understand the process and to develop a more efficient procedure. We cover both thermodynamic analysis and experimental validation. We found that high shear melt conditioning technology enhances the typically slow nucleation and growth of the dense primary intermetallics, speeding up their sedimentation and allowing a faster removal of Fe from the melt by simple gravity sedimentation. It also promotes the formation of smaller and more compact Fe-rich intermetallics, allowing an increased volume fraction recovery and mitigating their effect of being present in the final castings. The technology is not limited to batch processing, with a 90% efficiency, but can also be applied to continuous melt treatment of aluminium scrap, with currently 60% efficiency, and could be combined with other solid–liquid separation techniques to increase the purification efficiency even more.

Keywords: aluminum alloy; melt treatment; intermetallics; nucleation; sedimentation; purification; recycling

Citation: Lazaro-Nebreda, J.; Patel, J.B.; Al-Helal, K.; Gao, F.; Stone, I.; Chang, I.T.H.; Scamans, G.M.; Fan, Z. De-Ironing of Aluminium Alloy Melts by High Shear Melt Conditioning Technology: An Overview. *Metals* **2022**, *12*, 1579. https://doi.org/10.3390/met12101579

Academic Editor: Marcello Cabibbo

Received: 31 July 2022
Accepted: 19 September 2022
Published: 23 September 2022

1. Introduction

The interest in aluminium alloys from the automotive and aerospace sectors has been continuously increasing in the last decades due to the weight reduction, compared to steel, and the high-performance possibilities that these materials offer [1]. However, the main source of aluminium alloys for industry is still mainly primary production [2,3].

Recycling of aluminium alloy scrap to produce the ingots to be used in foundries is beneficial from an economic and environmental point of view because it requires less energy and produces less CO_2 emissions compared with the manufacturing of primary aluminium ingots [4]. However, the problem of repeated aluminium scrap re-melting is the gradual accumulation of impurities, in particular Fe. The solubility of Fe is high in molten aluminium, but it is very low in the solid state. During solidification, this excess of Fe combines with the Al and other elements in the alloy and tends to form a variety of intermetallic compounds [5]. The shape and size of these intermetallics depends on multiple factors including the alloy composition, solidification process and thermal treatments, but overall, they have a negative effect on the microstructure and the mechanical properties of the aluminium alloy castings [6–8].

Typical solutions in industry to overcome this problem include the downgrading of the material to less demanding casting applications or the dilution with expensive primary aluminium, but these are not long-term solutions and none of them solve the problem of iron accumulation [9]. In the last decades, several approaches have been developed and

investigated to remove the iron from aluminium scrap alloys [10], including gravity [11], filtration [12], centrifugal [13] or electromagnetic forces [14], electrolysis [15], fractional solidification [16,17], electroslag refining [18,19] and flux refining [20].

Despite the potential of all those approaches to lower the Fe content in the purified fraction, their efficiency in removing iron from aluminium melts is still low, either because the process is very energy demanding, or too slow, beyond industrial acceptability, or it can only remove a small volume fraction of the accumulated impurities, so the investment does not cover the benefits. Among these methods, the one that is normally preferred due to its simplicity and relatively low cost is known as the precipitation of primary Fe-rich intermetallic compounds (P-Fe-IMCs) [10].

The precipitation method is based on the natural formation of these Fe-rich phases during solidification but when the melt is still at a temperature above the liquidus for the formation of the α-Al phase. These solid intermetallics have a density of about 3.2 g/cm^3 [5], and they have a natural tendency to settle in the melt due to their higher density compared to the liquid alloy (~2.3 g/cm^3). In order for this to happen, the content of Fe (and other elements such as Mn and Si) needs to exceed a certain content in the alloy, otherwise the Fe-rich intermetallics are formed only after the nucleation of the α-Al phase. In such cases, natural gravitational sedimentation is hindered by high viscosity and the separation, within this fractional solidification scenario, needs to be assisted by either centrifugation [16] or by external pressure [17].

That is the reason why, although the method is theoretically applicable to any alloy system, in practice, it is mainly applied to high Si Al-Si casting alloys, in which the presence of primary intermetallic phases becomes more natural. It those cases, the Fe is removed by the precipitation of heavy primary intermetallics, such as α_$Al_{15}(FeMn)_3Si_2$ or β_Al_5FeSi, when the melt is maintained for long enough at a temperature above the α-Al formation [21–23]. The main disadvantage of this method is that the formation and growth of these intermetallics is very slow, and the separation process requires long residence times to be fully effective [5,23], which makes it impractical for large scale operations. It is known that primary Fe-rich intermetallics tend to nucleate on the wetted side of oxide films entrained in aluminium alloys [11,24,25]. However, these oxides are normally agglomerated and not well dispersed within the melt, and this hinders the nucleation and delays the growth of the intermetallics and their precipitation [26]. The addition of other elements, such as Mn or Cr, is widely used to promote the formation of larger and more compact Fe-rich phases, thus increasing separation efficiency [27–29]. The tendency of Al-Si-Cu alloys to form primary Fe-rich intermetallics can be approached in terms of the sludge factor (SF), a parameter that can be calculated by the empirical Equation (1). Some studies reported a minimum of SF~1 for the precipitation of P-Fe-IMCs [30].

$$SF = (1 \times wt.\%Fe) + (2 \times wt.\%Mn)\ (3 \times wt.\%Cr) \quad (1)$$

However, the addition of secondary elements such as Mn or Cr, apart from being an extra step in the process with its associated costs, should be kept as low as possible to maintain a sustainable recyclability of the material and prevent the accumulation of excess in the alloy exceeding the alloy limits or forming other intermetallics [31]. The search for alternatives to improve the method becomes necessary.

The use of high shear melt conditioning (HSMC) technology [32–34], developed within the Brunel Centre for Advanced Solidification Technology (BCAST) at Brunel University London, can overcome some of these problems. It can fragment and disperse the large oxide films and clusters into very fine and uniformly distributed individual particles [35,36], thereby enhancing the nucleation of intermetallic phases [37], and at the same time maximize the effect of the alloy chemistry so no additions in excess are required to enhance the formation of Fe-rich phases. In this paper, we present an overview of the progress made during the LiME Hub program to increase our understanding of the P-Fe-IMC precipitation–separation method and also to evaluate the effect of the developed HSMC

technology to improve the efficiency of iron removal from aluminium melts, so the process becomes more practical and sustainable to be implemented in the recycling industry.

2. Methodology

2.1. Aluminium Alloy Analysis by Thermodynamic Modelling

The purification of Al melts based on the precipitation of P-Fe-IMC intermetallics is a challenging process because it requires fine control of the temperature for the formation of the primary phases and an understanding of the limits on iron removal associated with each alloy composition. To evaluate whether an alloy with high Fe content will present P-Fe-IMCs, and the temperature range at which they form, the use of computational thermodynamic analysis tools becomes necessary. The Pandat software (Pandat with Pan Al Database Version 2021, CompuTherm LLC, Middleton, WI, USA) [38,39] was used during the investigations.

Figure 1 shows some examples of phase diagrams versus Fe content for four typical aluminium alloys used in industry, such as the 6082 (Figure 1a), 5182 (Figure 1b), 6016 (Figure 1c) and the A380 alloys (Figure 1d). The first three, wrought alloys, do not exhibit the presence of primary Fe-rich intermetallic compounds for an Fe level below 1%Fe, while the Fe limits in these alloys are typically much lower (Table 1). The maximum Fe level in recycled material from these alloys is typically far below 1%, and when it reaches higher values of Fe, it also exhibits the presence of other elements, such as Si, Mn, Cu and Zn, above the specification limits [40]. Therefore, the purification method based on P-Fe-IMC precipitation is not of practical use for wrought aluminium alloys as it is not able to operate at the relatively low Fe levels that these alloys require. The addition of Mn or Cr also does not work in this case because the amounts needed would also exceed the maximum allowed in the alloy specifications.

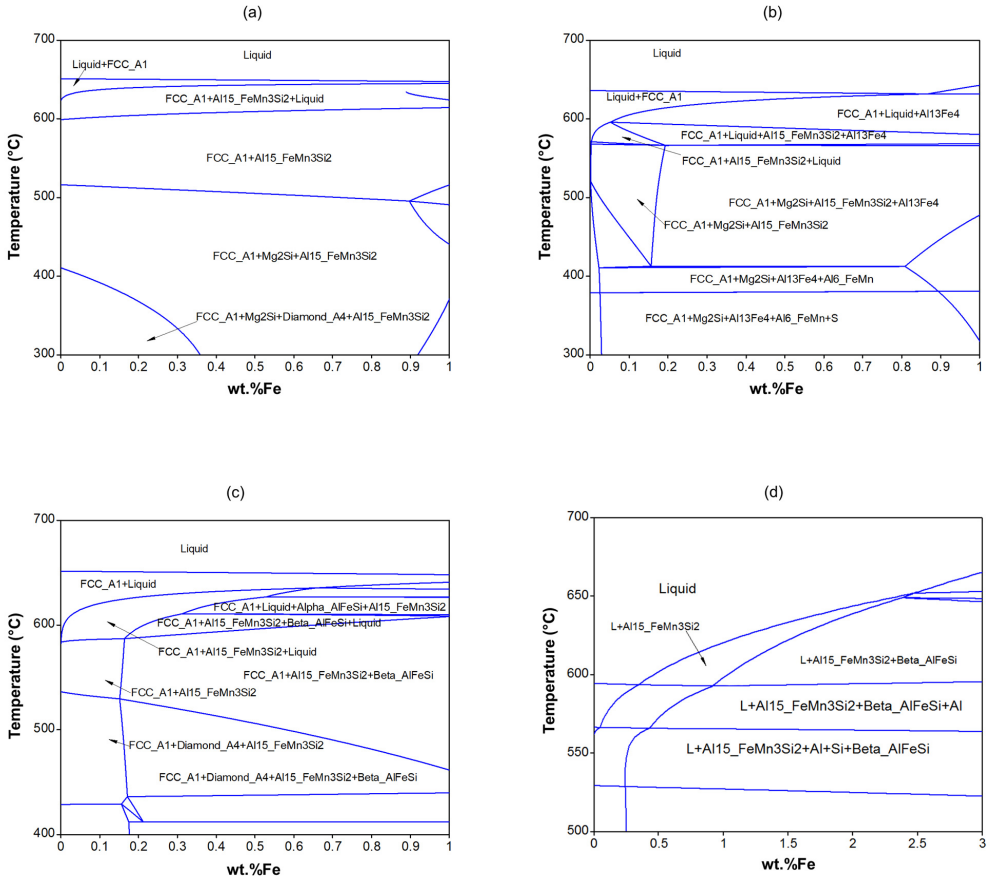

Figure 1. Equilibrium phase diagram versus Fe content for three wrought aluminium alloys and one aluminium cast alloy: (**a**) 6082-xFe; (**b**) 5182-xFe; (**c**) 6016-xFe and (**d**) A380-0.2Mn-xFe.

Table 1. Minimum level to form P-Fe-IMCs and commercial composition limits for the different alloys shown in Figure 1.

Alloy	Min %Fe to Form P-Fe-IMCs	Max %Fe Allowed in the Alloy
6082	1.15	0.5
5182	0.85	0.35
6016	1.25	0.5
A380	0.35	1.2

In practice, the P-Fe-IMC precipitation method turns out to be effective mainly to purify relatively high Si Al-Si cast alloys. Besides the effect of Si on lowering the temperature at which the α-Al phase appears, which increases the chances of other phases nucleating beforehand, for a given Fe content in the alloy there is a minimum Si level to make it thermodynamically possible to observe the primary β_AlFeSi phases that could settle in the melt [41,42]. Very low values of Si in Al cast alloy, such as, for example, the case of the A201 alloy, leads to the same problem mentioned before for the wrought alloys.

Because of this, the investigations on this method focused on alloys such as A380/LM24 or LM27, for which the Si content is between 6 to 9% and the tolerance to Mn relatively high. Figure 1d shows how the A380-0.2Mn aluminium cast alloy exhibited primary Fe-rich intermetallic compounds at much lower Fe content, which correspond to the α_$Al_{15}(FeMn_3)Si_2$ phase when the Fe level is between 0.35 and 0.95% and a mixture of the α_$Al_{15}(FeMn_3)Si_2$ and the β_Al_5FeSi phases above 1%Fe, The presence of Mn in this alloy plays an important role in the appearance of such P-Fe-IMCs and the effectiveness of the purification method [43,44] as it will be discussed later.

The initial studies of the A380-xMn-yFe alloy system to understand the potential and limitations of the purification method were conducted computationally, although with some experimental validation [31,44]. Later studies involved the use of melt conditioning to study its effect in the separation process [45–47] as well as the effect of solidification processing conditions [48]. Table 2 presents an example of two of the alloys studied, and for which we will be presenting some key results later in the paper. These values aim to reproduce typical compositions that could be found in this alloy system when dealing with real scrap [5]. To this end, the Al-80Fe and the Al-60Mn master alloys were used to increase the Fe and Mn levels in the aluminium melts.

Table 2. Typical composition (wt.%) spec. of A380 alloy and two variations used to simulate Fe and Mn contamination.

Alloy	Si	Fe	Mn	Cu	Mg	Zn
A380 spec	7.5–9.5	<1.3	<0.5	3.0–4.0	<0.1	<3.0
Alloy 1	8.22	2.05	0.22	3.32	0.06	1.93
Alloy 2	8.31	0.98	1.04	3.46	0.05	1.97

Currently, the focus of our research is also on the applicability of the methods on real aluminium scrap. In a recent publication [49], we covered the use of the de-ironing method on aluminium alloy recovered from the Zorba Cast fraction of shredded end-of-life vehicles, with a composition like the LM27 alloy, and the preliminary results look promising.

2.2. The High Shear Melt Conditioning Technology Setup for De-Ironing

Figure 2 shows a schematic illustration of the high shear melt conditioning technology (HSMC) prototype developed at BCAST [34] during the project for the purification of aluminium alloy melts. It consists of three parts. The first part of the setup is the processing chamber and it is the core of the technology. It consists of a heated vessel containing a ~6 kg graphite crucible with a baffle to separate the vessel into two sections, one (~5 kg) for receiving the molten scrap and another (~1 kg) for melt conditioning using a rotor-stator unit [33]. The size and design of the chamber and the processing section account for maximizing the level of melt shear rate and mass flow as these are restricted to the close

vicinity of the mixing head [50]. The implementation of the technology on large vessels requires an increase in the size of the unit and still further analysis, by computational fluid dynamic (CFD) modelling [51] and experimental validation [52], on the fluid flow and key features of the high shear processing. At this stage, the oxide agglomerates in the melt are finely dispersed because of the intensive melt shearing [35–37] and the composition and temperature are quickly homogenized by the strong macroscopic flow provided by the rotor-stator unit.

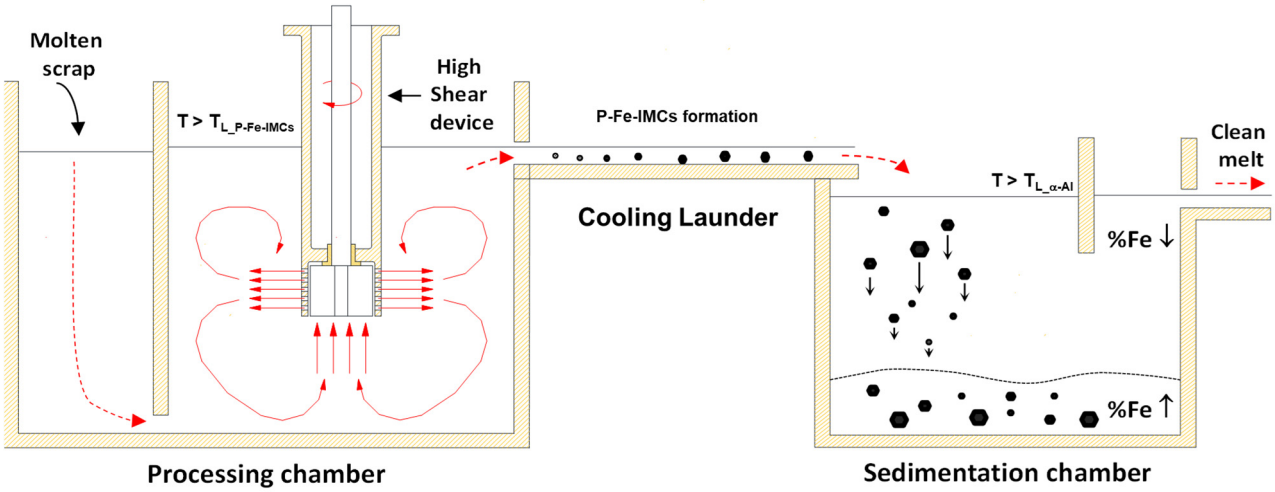

Figure 2. Schematic of the high shear melt conditioning (HSMC) technology for batch and continuous processing of aluminium alloy scrap for the removal of iron from the aluminium melts.

The melt in the processing chamber is kept at high temperature, above the formation of primary intermetallic phases ($T_{L\_P\text{-}Fe\text{-}IMCs}$), to prevent early sedimentation. For the case of the A380 alloy (Figure 1d), this implies at least 650 °C for an Fe content up to 2%. The rotor-stator unit is operated at high speed, typically at 3000 rpm and for a period of at least 1 min [53]. The time needed to ensure an effective processing increases with the vessel size [54], as more melt needs to be treated. However, the mass flow through the rotor stator depends linearly on the rotor speed [55] and also changes with the rotor-stator configuration [56], so the minimum processing time can be controlled by varying these parameters.

Once the melt is processed, there are two options to operate with the technology. On the one hand, the chamber can be tilted to pour the melt to another crucible in a furnace where is to be held and further processed as required (batch processing). On the other hand, more aluminium melt can be poured into the inlet of the processing chamber (continuous processing), so there is an outlet flow that goes directly into a cooling launder, where the melt temperature is reduced as it flows down. The function of this second stage of the setup is to decrease the temperature from above the liquidus for the appearance of primary phases down to a temperature above the liquidus for the α-Al phase, i.e., cooling the melt but not allowing it to start solidifying. It is during this stage that the nucleation and growth of the Fe–rich intermetallic compounds are supposed to occur. The design and configuration of this stage need to be carried out specifically for the temperature range that needs to be covered, which is intrinsic to the aluminium alloy composition under consideration. To this end, the use of CALPHAD tools, such as the Pandat software mentioned in previous section, becomes necessary as shown in Figure 1.

From the launder, the melt is transferred into the last stage of the setup, denoted as the separation chamber; a heated vessel made from a graphite crucible like the processing chamber. The purpose of this chamber is to keep the melt at a controlled temperature and prevent the solidification, by operating at least 5 to 15 °C above the liquidus temperature for the formation of the α-Al phase ($T_{L\_\alpha\text{-}Al}$). For the case of the A380/LM24 alloy, this temperature is typically around 600 °C but increases to 610 °C for the LM27 alloy sys-

tem [49] due to the lower Si content. Isothermal holding allows the intermetallics formed in the launder to settle directly to the bottom when they reach the separation chamber. The main advantage of this configuration is that "clean" material, with low levels of Fe, can be directly collected from the top of the sedimentation chamber, or from the outlet when operated in continuous mode. The chamber includes baffles to ensure that the incoming particles remain inside, quickly settling, and are not carried out with the outlet flow. The particles accumulated in the bottom of the chamber can be either drained in situ or removed once the processing has finished.

3. Results and Discussion

3.1. Theoretical Prediction of Fe-IMC Formation by Pandat Phase Diagram Analysis

3.1.1. The Effect of Fe Accumulation in the A380 Aluminium Alloy

Figure 3a presents a more in-depth analysis of the phase diagram for the A380 alloy, with 0.2%Mn, as a function of the Fe content presented in Figure 1d. It can be observed that as Fe increased so did the temperature at which the primary phases appeared. This widens the temperature window for the formation of the primary phases, as the α-Al phase forms at 595 °C independently of the initial %Fe. For example, for an initial 1%Fe in the alloy the primary intermetallics, mostly α_$Al_{15}(FeMn)_3Si_2$, are expected to form in a narrow 25 °C range, between 620 and 595 °C, while for an initial 2%Fe, a combination of α_$Al_{15}(FeMn)_3Si_2$ and β_Al_5FeSi will form on a wider 51 °C range, between 646 and 595 °C. For an initial level of 3%Fe, a more complex mixture of P-Fe-IMCs (including also the α_AlFeSi phase [41]) is expected to form in a 77 °C range, from 667 to 595 °C. It is clear that as Fe level increases it becomes more likely to observe the presence of P-Fe-IMCs and easier to operate on a sufficiently wide temperature window.

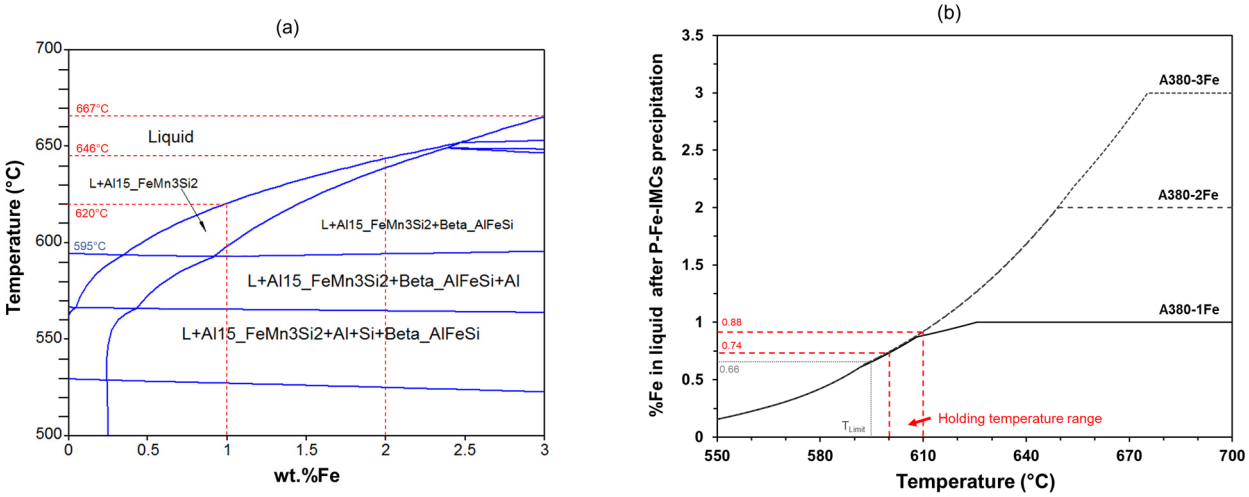

Figure 3. (**a**) Equilibrium phase diagram of the A380-0.2Mn alloy versus Fe; (**b**) level of Fe remaining in the liquid phase as function of temperature for three initial Fe levels as the P-Fe-IMCs form during solidification.

As the primary phases formed, the concentration of Fe in the remaining liquid alloy decreased. Figure 3b shows this variation as a function of the alloy temperature for three different initial Fe contents. Vertical and horizontal lines have been included to mark the key points in the graph. For high temperatures, the differences are clear, but the final Fe level expected in the liquid was almost the same in the three cases when the melt was at a holding temperature below 610 °C. The minimum value possible, at T = $T_{L\alpha\text{-}Al}$, was 0.66%Fe, although holding at that low temperature would not be practical because small variations would lead to partial solidification of the α-Al and the intermetallic movement would be hindered. For the purification method to be more effective, the melt temperature should be held at least between 600 and 610 °C. In this case, the expected Fe level in the liquid would range between 0.74 and 0.88%, with an average value of 0.81%. This value

falls below the maximum limit of the A380 alloy (Table 2) and opens the possibility of processing contaminated A380 alloy, i.e., Fe > 1.3%, without the need of Mn addition. In practice, the experimental values tended to be a bit higher (~1%Fe) when holding in this temperature range, because the sedimentation process required a long time, but even then, they were still within the alloy specifications [23].

3.1.2. The Effect of Mn Additions on an Fe Contaminated A380 Aluminium Alloy

Despite the possibility of avoiding the use of Mn additions for the purification of the A380-0.2Mn alloy to an acceptable Fe level (0.8–1.0%), if an Fe level below 0.8% is required, then the melt needs the addition of Mn to promote the formation of more Fe-rich intermetallics. To help understand this, Figure 4a shows how the phase diagram in Figure 3a varies with the increment of Mn in the alloy. The variation of Mn does not affect the α-Al phase formation temperature and, therefore, the holding temperature for the formation and separation of the intermetallic phases can be kept the same (600–610 °C).

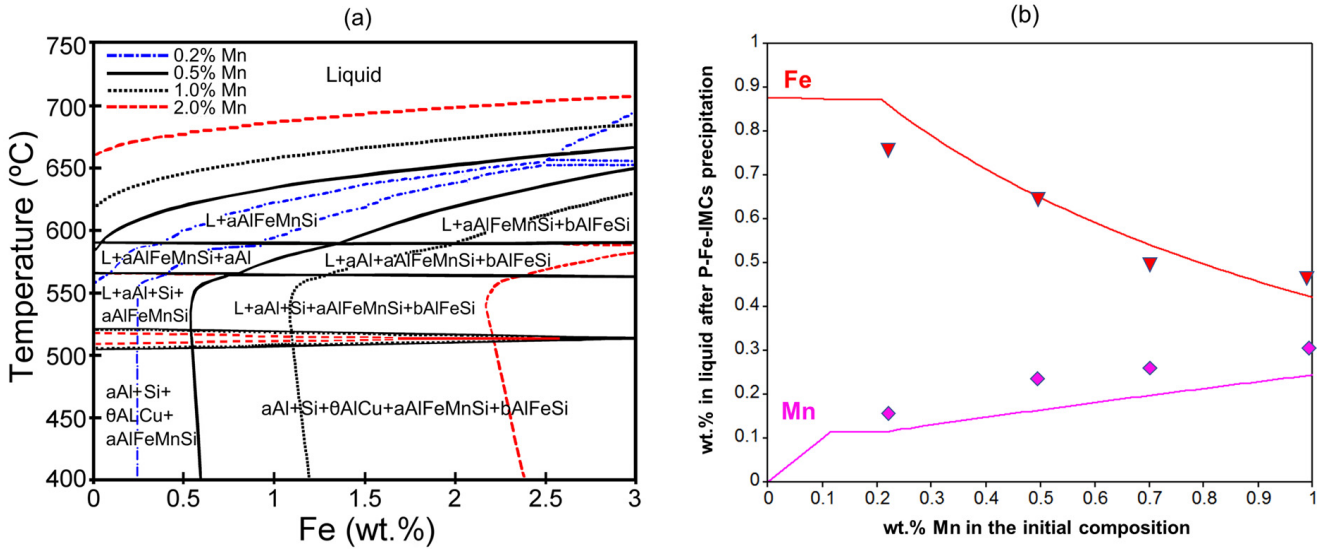

Figure 4. (**a**) Equilibrium phase diagram of the A380 alloy versus Fe for different Mn additions. Reprinted with permission from ref. [44]. Copyright 2022 Elsevier; (**b**) Fe and Mn in liquid A380-1Fe alloy versus Mn content when held at 610 °C. Lines are predictions from Pandat software and the points are experimental values obtained at 605 ± 5 °C.

Mn addition widens the temperature range for the precipitation of the primary phases by increasing the temperature at which they start appearing. For the case of an A380 alloy with 1%Fe, this happened at 620 °C when the Mn level was around 0.2%, at 634 °C for 0.5%Mn, at 652 °C for 1%Mn and at 687 °C when the Mn content was 2%, thus, increasing the temperature window from ~20 °C to ~90 °C. Moreover, increasing Mn in the alloy facilitates the appearance of the α_$Al_{15}(FeMn)_3Si_2$ phase to the detriment of the β_Al_5FeSi phase. When the Mn/Fe ratio in the alloy is below 0.5 we can expect both α and β phases with dominance of the β phase. When Mn/Fe exceeds 0.5 the α phase becomes more dominant and when Mn/Fe > 1 the β_Al_5FeSi phase is suppressed and only the α_$Al_{15}(FeMn)_3Si_2$ phase is expected to appear during the solidification [57,58]. The α_$Al_{15}(FeMn)_3Si_2$ phase is more compact and rounded than the β phase and, therefore, an adequate Mn addition can be used to control the microstructure of the castings and improve the mechanical properties [58–60]. However, the change of morphology of the P-Fe-IMCs with the increased Mn/Fe ratio also facilitates their separation as the compact α particles become larger and can settle faster.

Figure 4b shows the expected effect of Mn addition on the Fe and Mn levels in the liquid phase when the alloy is maintained at 610 °C. In this particular case, the Fe level can be theoretically reduced down to 0.42%Fe when Mn is added up to 1%, with experiments

showing good agreement with an Fe decrease down to 0.47%. In the process, Mn is also consumed in the formation of the α_$Al_{15}(FeMn)_3Si_2$ phase and the final Mn level in the liquid is also much lower than the initial addition level. However, experimental trials with these additions showed that, in practice, the remaining Mn level in the liquid phase tended to be underestimated by the software predictions. Experimental content after purification of a A380-1Mn-1Fe alloy showed a Mn content of 0.32% [44] when the Pandat software predicted 0.24%Mn. This highlights the importance of an adequate thermal analysis consideration and not using Mn in excess to maintain a sustainable iron removal process. Furthermore, it has been reported that the increase in Mn in the alloy balances the content of Fe and Mn in the α_$Al_{15}(FeMn)_3Si_2$ phase towards more Mn and less Fe [61], thus limiting the Fe removal efficiency [58].

3.2. Experimental Assessment of Fe-IMC Formation

3.2.1. Effect of HSMC on the Nucleation Kinetics

The nucleation of the primary Fe-rich intermetallics exhibits a high undercooling, which facilitates the suppression of their formation if the cooling rate is high enough [62]. This is obviously not desired as the aim is to produce the P-Fe-IMCs as early as possible, so they have more time to settle. Applying HSMC enhances the formation of the primary intermetallic by reducing the undercooling and facilitating their earlier formation [36]. To study the solidification behavior, batches of melts (~1 kg) were held at 720 °C and then processed with the HSMC at 3000 rpm for 10 min. The conditioned melt was then poured into a set-up consisting of a preheated small crucible (~0.3 kg) covered with thermal insulation to control the cooling rate [63]. A 0.5 mm K-type thermocouple was immersed in the melt right after pouring and fixed at the center of the melt. The temperature was acquired through a datalogger at 100 Hz. Sampling without HSMC was also collected as a reference.

Figure 5 shows some examples of cooling curves for the A380 alloy with different Fe and Mn contents and solidified and different cooling rates by varying the thermal insulation around the crucible. The cooling rate in each case was calculated from the slope of the curve at the beginning of the process, in the range from 700 to 650 °C. It can be observed that the curves present an inflex point somewhere between 650 and 600 °C, which corresponds to the nucleation of the primary intermetallics [61,64].

For the A380 alloy with 2%Fe and 0.2%Mn (Figure 5a), the primary phases are expected to nucleate at 646 °C. However, the natural undercooling moves this point to 619 °C for the reference material when cooled at −0.15 K/s, thus exhibiting a 27 °C difference. The nucleation temperature for the primary intermetallic phase after HSMC increases to 635 °C, with only 11 °C undercooling. Similar low undercooling can be found in the reference melt but when using a much lower cooling rate [61], which highlights the difficulties for practical implementation and the need for enhancement methods.

These differences become clearer as the cooling rate increases, so the formation temperature for the P-Fe-IMCs decreases [57,58,62]. For the A380 alloy with 1%Fe and 1%Mn, the primary α_$Al_{15}(FeMn)_3Si_2$ phase was expected to form at 652 °C but it was observed at 624 °C for the reference melt when cooled at −0.3 K/s (Figure 5b) and at 603 °C when cooled much faster at −3.2 K/s (Figure 5c). After the use of HSMC, the nucleation temperatures increased to 642 and 622 °C, respectively, thus reducing the undercooling more than 15 °C regardless of the cooling rate, making it more practical for industrial implementation. An earlier formation gives the Fe-rich intermetallics more time to grow and start settling in the melt during the cooling process before reaching the holding temperature.

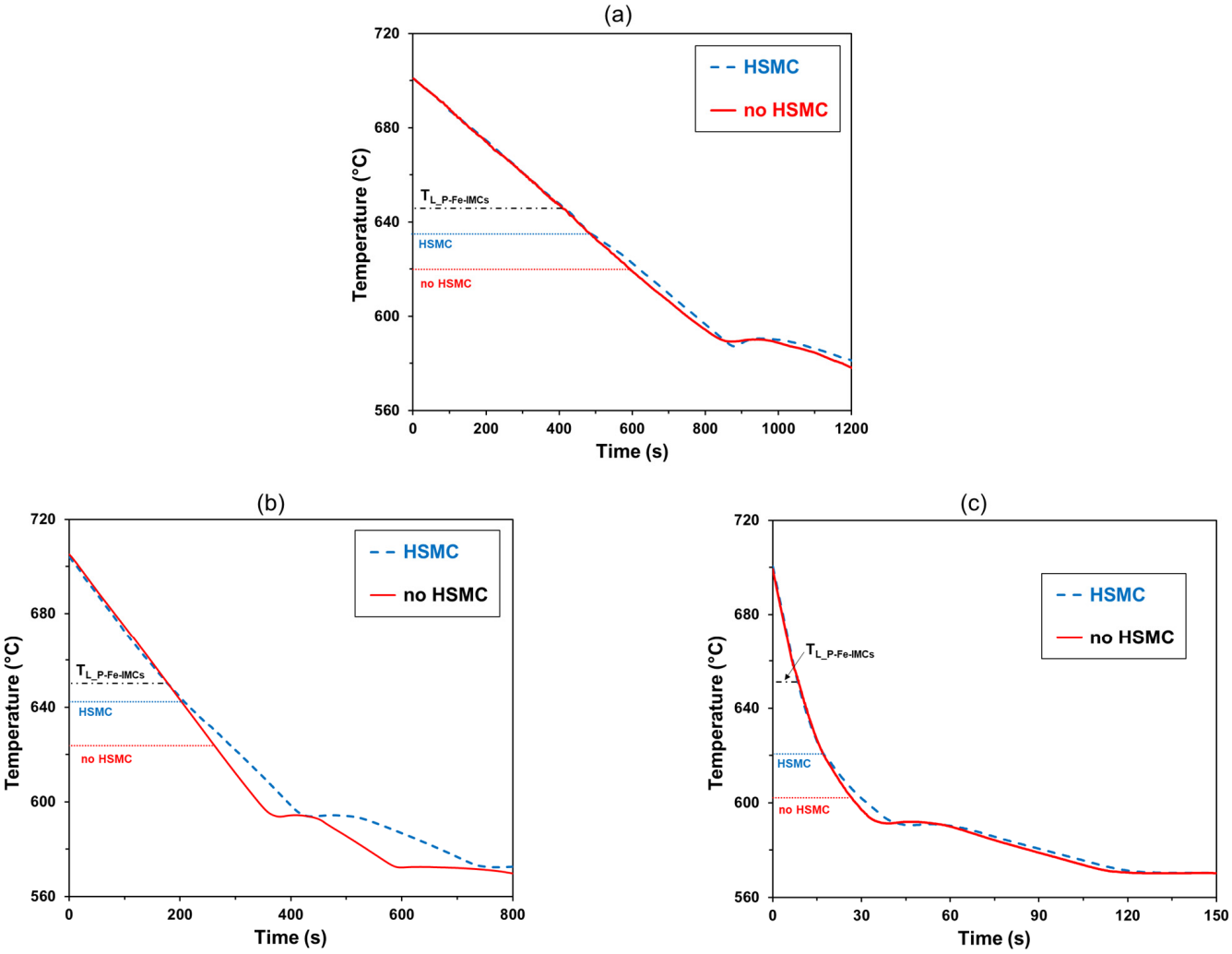

Figure 5. Cooling curves of A380 aluminium melts before and after HSMC at 700 °C for 10 min. (**a**) Alloy 1 at −0.15 K/s; (**b**) Alloy 2 at −0.3 K/s; (**c**) Alloy 2 at −3.2 K/s.

3.2.2. Effect of HSMC on the Size and Shape of Fe-IMC

Figure 6 shows the effect of HSMC on the microstructure of the A380 alloy containing 0.2%Mn and 2%Fe (Alloy 1) in the solidified samples before and after HSMC. For the reference material, without HSMC, the micrograph in Figure 6a shows both types of intermetallics, but more fractions of the large and elongated β-phase (309 ± 109 µm) and only a few branched α-phase intermetallics (32 ± 16 µm) were formed. After the application of HSMC (Figure 6b), the β-phase became refined in size (224 ± 113 µm) and became less dominant and more compact and bigger α-phase intermetallics (53 ± 25 µm) could be observed in the microstructure [37]. The circularity of the particles (*Circ.*) can be calculated by Equation (2), where A is the area of the particle and P its perimeter. For the case of Figure 6, the circularity changed from 0.10 ± 0.04 to 0.17 ± 0.05 for the β-phase and from 0.71 ± 0.26 to 0.74 ± 0.17 for the α-phase.

$$Circ. = 4\pi A / P^2 \quad (2)$$

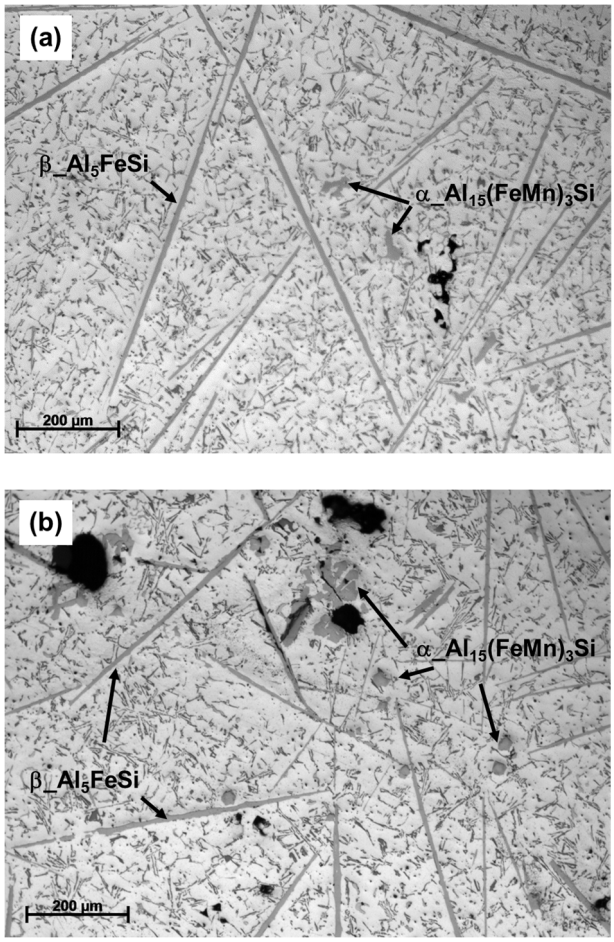

Figure 6. Optical micrographs showing the Fe-containing intermetallics in solidified A380-0.2Mn-2Fe alloy (**a**) without HSMC; and (**b**) after HSMC in the solidified samples.

Figure 7 shows the effect of HSMC on the microstructure of the A380 alloy containing 1%Mn and 1%Fe (Alloy 2) in the solidified samples before and after HSMC. In this case, for the reference material without HSMC (Figure 7a), the presence of high level of Mn ensured the formation of only the primary α_$Al_{15}(FeMn)_3Si_2$ phase, with an average size of 137 ± 15 µm. The application of HSMC increased the number density of the intermetallics (Figure 7b). It also reduced their size to 102 ± 21 µm but increased their circularity from 0.72 ± 0.15 before HSMC to 0.81 ± 0.12 after HSMC. This supports the idea of the dispersed oxide films acting as nucleation sites for the Fe-rich intermetallics [65]. The nucleation of the P-Fe-IMCs occurs progressively in bursts during cooling [66] due to the low content of active nuclei available in the melt, which leads to large and irregularly shaped particles. The dispersion of the oxide biofilms naturally occurring in the melt facilitates the presence of more active nuclei, which results in a more explosive nucleation, with a lower growth but leading to a more compact final shape [67].

3.3. Effect of HSMC on the Sedimentation of the P-Fe-IMCs

3.3.1. Effect during Direct Solidification to Room Temperature

Figure 8 shows the level of Fe along the vertical profile for the A380-0.2Mn-2Fe alloy, with and without HSMC, solidified inside a crucible from 700 °C directly to room temperature at a similar cooling rate (−0.15 K/s). A dashed vertical line has been included to indicate the initial Fe content and a dotted line and shadowed region to indicate the expected level of Fe in the melt at 605 ± 5 °C, according to the values shown in Figure 3b. A gradient was observed in both cases, which highlights the formation and partial sedimentation of the primary phases during the cooling. This gradient was clearly higher on

the HSMC material because the nucleated particles were less elongated (Figure 6b), and their earlier formation (Figure 5a) gave them time to settle during the cooling process while the alloy was still in the liquid.

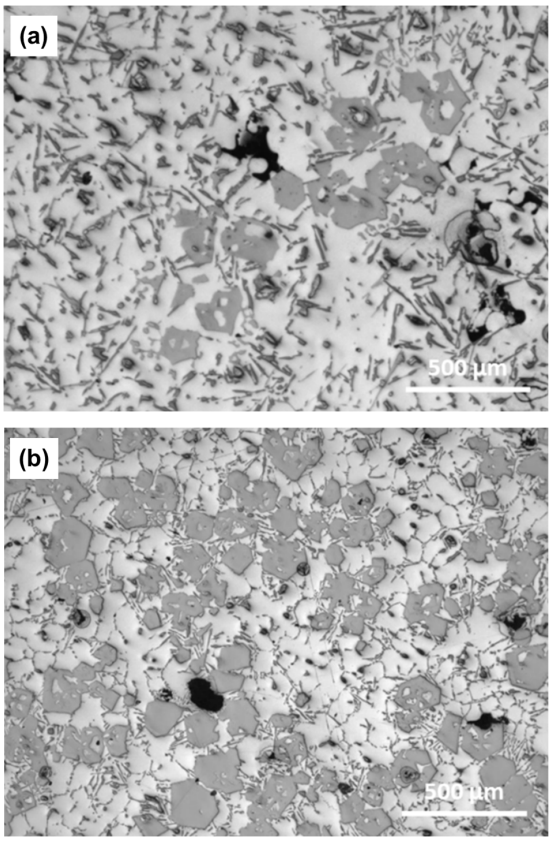

Figure 7. Optical micrographs showing the Fe-containing intermetallics at the bottom of a solidified A380-1Mn-1Fe alloy (**a**) without and (**b**) with HSMC.

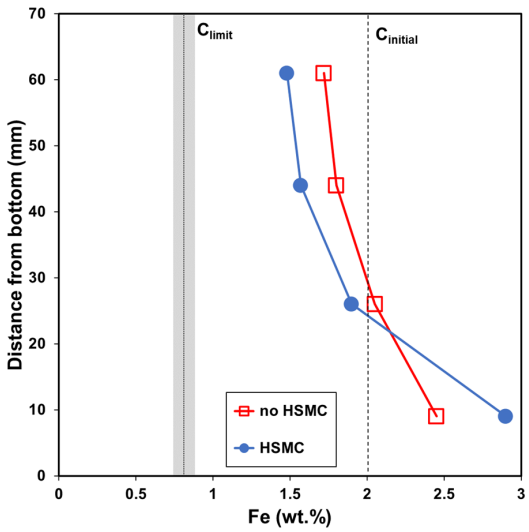

Figure 8. Effect of HSMC on the Fe level along the vertical profile for a A380-0.2Mn-2Fe alloy solidified in a preheated crucible from 700 °C to room temperature and at −0.15 K/s cooling rate. Vertical lines indicate the Fe level at the beginning of cooling ($C_{initial}$) and the expected (C_{limit}) after precipitation of all the P-Fe-IMCs.

Based on the initial and final values reached from this analysis and the expected results from the Pandat software analysis, we can define a process efficiency. On the one hand we

have a purification efficiency with respect to composition (η_{Comp}) that can be defined using Equation (3), where $C_{initial}$ is the initial Fe level in the melt, C_{limit} is the expected Fe level at 605 °C and C_{top} refers to the Fe level in the upper part of the sample, obviously lower than $C_{initial}$ and different in each case (with and without HSMC). This efficiency increases from 26 to 46% after HSMC.

$$\eta_{Comp} = \frac{C_{initial} - C_{top}}{C_{initial} - C_{limit}} \quad (3)$$

On the other hand, we can define an efficiency based on the volume fraction of material purified, η_{Vol}, by using Equation (4), where V_{total} is the sample volume and V_{clean} is the fraction of material with a Fe level below the initial content. This efficiency increases from 58 to 67% after HSMC.

$$\eta_{Vol} = \frac{V_{clean}}{V_{total}} \quad (4)$$

3.3.2. Effect during Holding at Constant Temperature in the Liquid

Figure 9a shows the Fe level along the vertical profile when a reference A380-1Mn-1Fe alloy melt was cooled from 700 °C at a −0.3 K/s cooling rate and poured inside a cylindrical temperature c ontrolled vessel to be kept at 605 ± 5 °C for different times to allow the P-Fe-IMCs to settle. The sedimentation was slow, and the process took up to 10 to 15 min to be completed. The refined melt at the top of the vessel showed a level of 0.47%Fe, which is very close to the thermodynamic calculations using Pandat software (C_{limit} = 0.42%Fe). This gives an efficiency in terms of composition of η_{Comp} = 91%. The concentration at the bottom obviously increased as the P-Fe-IMCs accumulated with time. The corresponding vertical profiles of the melt that were subjected to HSMC before being cooled at same rate and poured into the holding vessel are shown in Figure 9b. In this case, the composition gradient from the top to the bottom of the vessel was more pronounced and the sedimentation process was completed much faster. The purification efficiency in terms of volume fraction was similar in both cases, with a η_{Vol} = 75% before and η_{Vol} = 77% after HSMC.

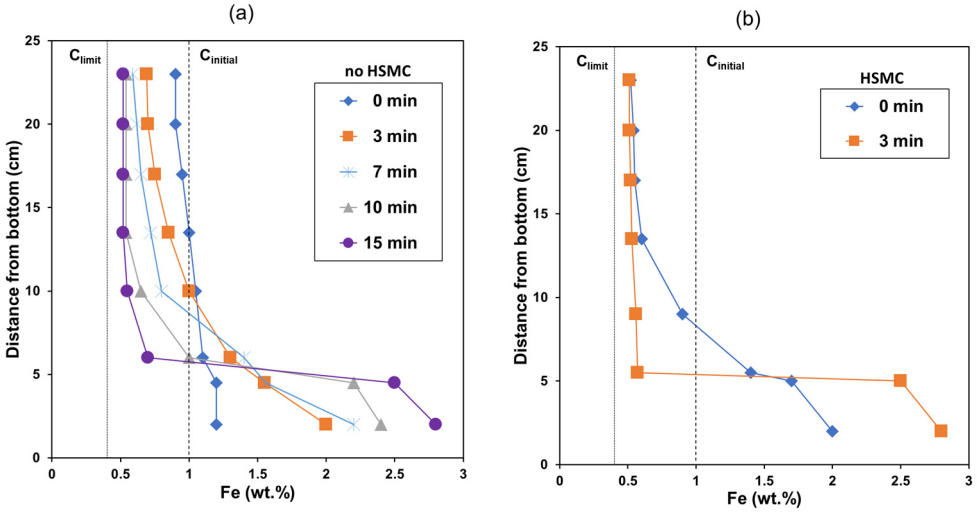

Figure 9. Sedimentation of Fe-rich intermetallics in A380-1Fe-1Mn alloy melt during holding at 605 °C for different times in a preheated cylindrical vessel. (**a**) Without melt treatment and (**b**) after using the HSMC technology in batch processing mode.

The velocity (v_s) at which solid spherical particles settle in the liquid alloy can be expressed by Equation (5) (Stoke's Law) [68], where g is the acceleration due to gravity, ρ_{sol} and ρ_{liq} are the density of the solid particle and the fluid respectively, ϕ is the diameter of the particle and μ is the viscosity of the liquid Al (1.4×10^{-3} Pa s [44]).

The larger the form of the intermetallic particles, the faster they settle in the melt, and therefore the refinement of particle size produced by HSMC should in fact decrease the

sedimentation if we stick to the estimation from Equation (5). However, the shape of the particle also needs to be considered in this case. For the case of non-fully spherical solid particles, a recent study [69] has shown that the settling velocity (v_s^*) can be approached by Equation (6), where g_e, K_ϕ, K_f and v_L are correction factors accounting for the particle shape and the fluid flow effects on the particle movement. The earlier formation of the intermetallics after HSMC (Figure 5b) and the fact they are more rounded and compact (Figures 6b and 7b), facilitates the sedimentation process and explains the higher settling velocity in the HSMC melts.

$$v_s = \frac{\left(\rho_{sol} - \rho_{liq}\right)}{18\mu} g\phi^2 \quad (5)$$

$$v_s^* = v_s \frac{g_e K_\phi}{K_f} + v_L \quad (6)$$

3.4. Implementation of HSMC De-Ironing in Continuous In-Line Processing

The operation of the technology in continuous or semi-continuous mode is more practical for industrial purposes as it facilitates the use of smaller configurations for a faster processing of the alloy regardless of the quantity of melt required. However, the implementation in continuous process requires fine control of the setup (Figure 2) to guarantee an adequate temperature gradient in the launder to start forming the intermetallics and a precise control of the melt temperature in the sedimentation chamber as the melt flows through.

Figure 10 presents an example of the temperature gradient along the different parts of the prototype system during a test with a A380-1Mn-1Fe alloy melt at a melt flow rate of 4 Kg/min. Temperatures were taken in the processing chamber, at the beginning and end of the launder and inside the sedimentation chamber. Some fluctuations in temperature along the launder can be observed due to a still ineffective melt flow control in the current prototype that would be solved with an automatic pouring system. Apart from that, the temperature control was quite good in the processing and the sedimentation chambers. It was above the liquidus for the formation of P-Fe-IMCs in the processing chamber, to prevent precipitation of the intermetallics in this stage, and fell within the range of formation range along the launder to finally be maintained in liquid above α-Al formation temperature.

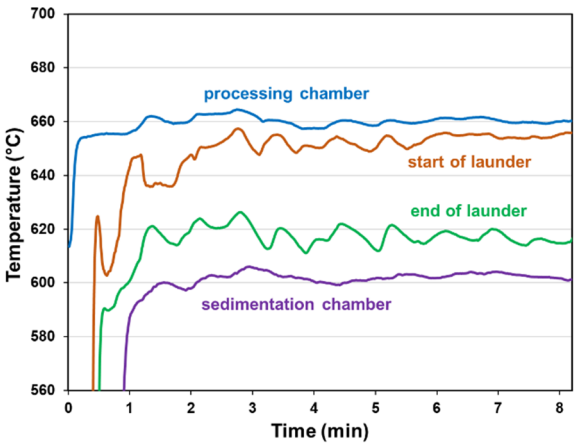

Figure 10. Temperature control in the different sections of the in-line HSMC de-ironing system while processing a A380-1Mn-1Fe alloy at a melt flow rate of 4 Kg/min.

The in-line configuration allows the collection of cleaned melt as it flows out of the sedimentation chamber and its transfer to another furnace where it can be heated up and further processed or be cast directly into ingots. Figure 11 shows the concentration of Fe in the liquid collected from the outlet as a function of time for tests carried out with and without applying HSMC in the processing chamber. Horizontal dashed lines were included to indicate the initial Fe concentration ($C_{initial}$), the lowest Fe level achieved during

batch processing (C_{batch}) and the theoretical limit for this alloy (C_{limit}) The melt collected after HSMC exhibited low Fe levels from the moment that there was an outflow, while the reference melt without HSMC started showing high Fe level that slowly decreased with time as the melt continued flowing out of the sedimentation chamber. This result demonstrates that with HSMC, the primary intermetallics form and grow at an earlier stage, along the launder connecting the two chambers. When the intermetallics reach the holding chamber they are bigger and tend to settle faster to the bottom, allowing the cleaner fraction to flow out. In contrast, when HSMC is not used, the primary intermetallic particles are more likely to form and grow after the launder cooling stage, i.e., once the melt reaches the holding chamber. In this case, the intermetallics are smaller and there is a competition between the growth and the sedimentation while the melt is passing through the chamber. Only with time, the particles get bigger and settle faster and the chamber starts delivering melt with a lower Fe content.

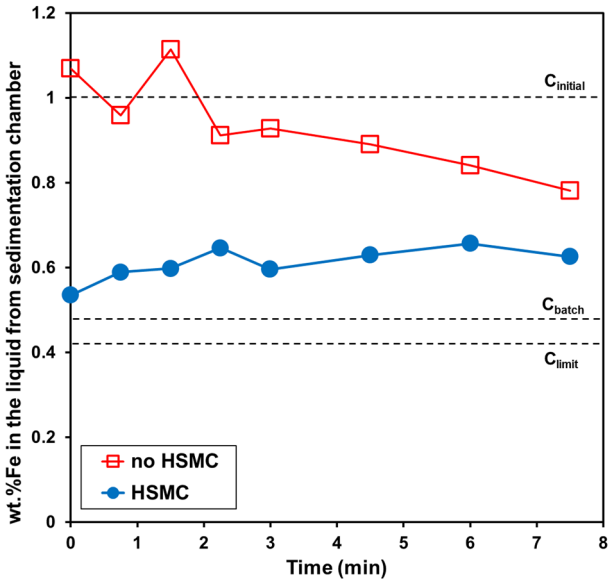

Figure 11. Level of Fe (wt.%) in the molten alloy collected from the sedimentation chamber as the molten metal starts to flow out (t = 0) from the sedimentation chamber at a continuous melt flow rate of 250 Kg/h.

With HSMC, the Fe level in the collected melt during the whole duration of the trial was quite stable, with an average Fe level of 0.66%, while for the reference melt the average Fe level in the collected melt was 0.87%. This represents an increase in process efficiency in terms of composition (Equation (3)) from 20 to 57% by using HSMC. The Fe levels during in-line processing are always slightly higher than the results obtained during in-batch processing for long holding time (0.47%Fe) and the process efficiency lower because, in this case, the particle sedimentation must also overcome the vertical melt flow out of the chamber (negative value of v_L in Equation (6)).

During these initial tests, no removal of the accumulated particles in the sedimentation chamber was performed, explaining the gradual increase for the HSMC line as shown in Figure 11. This issue represents a disadvantage for the current technology implementation because it limits the melt flow that can be processed, which is typically high in industry, but it will be solved in future modifications of the setup. Some of the possible solutions would be either increasing the size of the separation chamber or including a siphon system to remove the sedimented particles in situ.

For simplicity, the current in-line system has been only used to assess the separation of the intermetallics by gravity, but its configuration also allows it to be used in combination with other separation techniques. The options include the use of filters at the outlet of the separation chamber, or by coupling it with existing electromagnetic separation equipment [5,10] or even with gas bubbling for particle removal by flotation [68,70]. Using

this technological combination, the overall process efficiency could increase significantly and make it more attractive for the requirements of the aluminium recycling industry.

4. Conclusions

The purification of molten aluminium alloys by the precipitation of P-Fe-IMCs has been evaluated both from a theoretical and an experimental point of view and the high shear melt conditioning (HSMC) technology developed in BCAST has been used to evaluate its applicability to improve the iron removal process. The key conclusions obtained during the investigations can be summarized as follows:

- The precipitation method is only practical for high Si aluminium cast alloys because of their easy tendency to form P-Fe-IMCs within, or slightly above, the alloy specifications. The extension to other alloy systems would first require an increment of the limits for Fe, Si and Mn in the alloy specifications.
- The use of CALPHAD tools is essential to accurately predict the potential Fe removal from the contaminated aluminium melts and to estimate the operating temperature windows to achieve the best results.
- The Fe level in a contaminated A380 alloy can be theoretically reduced to ~1%Fe without the need of added Mn and regardless of the initial Fe content. However, if lower Fe levels are required, the use of Mn becomes necessary and can easily control the expected final Fe level in the purified melt.
- The precipitation and sedimentation of P-Fe-IMCs is a slow process which requires either a very slow cooling rate or long holding times to be effective.
- The HSMC technology before cooling enhances the formation of the primary Fe-rich intermetallics by reducing their undercooling, regardless of the cooling conditions. This produces an earlier sedimentation of the intermetallic particles in the melt during cooling and it is more practical for industry because it can reduce processing times and increase productivity.
- Moreover, the Fe-rich primary intermetallics produced after HSMC are more compact, something that facilitates their movement in the liquid aluminium and promotes a faster sedimentation.
- The HSMC technology is still at laboratory scale and limited to small amounts of melt, but ongoing research is focus on improving the applicability to large melts.
- Initial scale-up tests with the technology have demonstrated its feasibility for the continuous melt treatment of contaminated aluminum melts with a ~60% purification efficiency, which is below the ~90% efficiency obtained in batch. Further development is currently in progress to improve process efficiency.
- As a melt conditioning technology, the technology can also be used combined with other existing separation techniques (centrifugal, filtration, EM separation, etc.), therefore increasing the overall iron removal rate and efficiency.

5. Patents

A patent resulted from work carried out during the LiME Hub regarding the use of HSMC for purifying alloy melts: Fan, Z.; Ji, S.; Stone, I. Purifying and alloy melt. WO 2016146980 A1. https://www.freepatentsonline.com/WO2016146980A1.html (accessed on 22 July 2022).

Author Contributions: Conceptualization, J.L.-N. and J.B.P.; methodology, investigation, data analysis and validation, J.L.-N., J.B.P., K.A.-H. and F.G.; writing—original draft preparation, J.L.-N.; writing—review and editing, J.L.-N. and J.B.P.; supervision, project administration and funding acquisition, J.B.P., I.S., I.T.H.C., G.M.S. and Z.F. All authors have read and agreed to the published version of the manuscript.

Funding: The research was financially supported by EPSRC (UK) under grant number EP/N007638/1, by the European Commission under Grant No. 603577 and by Innovate UK under Project No.102797.

Institutional Review Board Statement: Not applicable.

Informed Consent Statement: Not applicable.

Data Availability Statement: The data presented in this manuscript is available on request from the corresponding author.

Acknowledgments: The authors would like to thank the support from the Brunel Centre for Advanced Solidification Technology (BCAST) at Brunel University, London, where this work was carried out.

Conflicts of Interest: The authors declare no conflict of interest.

References

1. Mondolfo, L.F. *Aluminium Alloys: Structure and Properties*; Butterworth-Heinemann: Oxford, UK, 1976. [CrossRef]
2. Lumley, R.N. *Fundamentals of Aluminium Metallurgy: Recent Advances*; Woodhead Publishing: Melbourne, Australia, 2018. [CrossRef]
3. Polmear, I.J. *Light Alloys Metallurgy of the Light Metals*; Butterworth Heinemann: Oxford, UK, 1995.
4. Green, J.A.S. *Aluminum Recycling and Processing for Energy Conservation and Sustainability*; ASM International: Materials Park, OH, USA, 2007.
5. Zhang, L.; Gao, J.; Damoah, L.N.W.; Robertson, D.G. Removal of iron from aluminum: A review. *Miner. Process. Extr. Metall. Rev. Int. J.* **2012**, *33*, 99–157. [CrossRef]
6. Ji, S.; Yang, W.; Gao, F.; Watson, D.; Fan, Z. Effect of iron on the microstructure and mechanical property of Al–Mg–Si–Mn and Al–Mg–Si diecast alloys. *Mater. Sci. Eng. A* **2013**, *564*, 130–139. [CrossRef]
7. Al-Helal, K.; Patel, J.B.; Fan, Z. Fe-rich Intermetallic Formation and Mechanical Properties of Recycled AA6111 Alloy Strips Produced by Melt Conditioning Twin Roll Casting. *JOM* **2020**, *72*, 3753–3759. [CrossRef]
8. Chmielewski, T.; Chmielewski, M.; Piatkowska, A.; Grabias, A.; Skowronska, B.; Siwek, P. Phase Structure Evolution of the Fe-Al Arc-Sprayed Coating Stimulated by Annealing. *Materials* **2021**, *14*, 3210. [CrossRef]
9. Dhindaw, B.K.; Aditya, G.S.L.; Mandal, A. Recycling and Downstream Processing of Aluminium Alloys for Automotive Applications. *Encycl. Renew. Sustain. Mater.* **2020**, *3*, 154–161. [CrossRef]
10. Zhang, L.; Damoah, L.N. Current Technologies for the Removal of Iron from Aluminum Alloys. In *Essential Readings in Light Metals*; Grandfield, J.F., Eskin, D.G., Eds.; Springer: Cham, Switzerland, 2016. [CrossRef]
11. Cao, X.; Campbell, J. Precipitation of primary intermetallic compounds in liquid Al-11.5Si-0.4Mg alloy. *Int. J. Cast Met. Res.* **2000**, *13*, 175–184. [CrossRef]
12. De Moraes, H.L.; De Oliveira, J.R.; Espinosa, D.C.R.; Tenorio, J.A.S. Removal of iron from molten recycled aluminum through intermediate phase filtration. *Mater. Trans.* **2006**, *47*, 1731–1736. [CrossRef]
13. Matsubara, H.; Izawa, N.; Nakanishi, M. Macroscopic segregation in Al-11mass% Si alloy containing 2 mass% Fe solidified under centrifugal force. *J. Jpn. Inst. Light Met.* **1998**, *48*, 93–97. [CrossRef]
14. Li, T.X.; Xu, Z.M.; Sun, B.D.; Shu, D.; Zhou, Y.H. Electromagnetic separation of primary iron-rich phases from aluminum-silicon melt. *Trans. Nonferrous Met. Soc. China* **2003**, *13*, 121–125.
15. Lu, H.; Yuan, W.; Xu, C.; Liu, Z.; Wu, B.; Zhang, Y. The development of 65KA three-layer electrolysis cell for refining of aluminium. *Light Met.* **2004**, 303–305.
16. Guo, L.; Wen, X.; Bao, Q.; Guo, Z. Removal of Tramp elements within 7075 Alloy by Super-Gravity Aided Rheorefining Method. *Metals* **2018**, *8*, 701. [CrossRef]
17. Venditti, S.; Eskin, D.; Jacot, A. Fractional Solidification for Purification of Recycled Aluminium Alloys. In *Light Metals*; Springer: Cham, Switzerland, 2020; pp. 1110–1118. [CrossRef]
18. Mohanty, B.P.; Subramanian, S.; Hajra, J.P. Electroslag refining of commercial aluminium. *Trans. Indian Inst. Met.* **1986**, *39*, 646–651.
19. Wang, J.; Chen, C.; Sun, B. Effects of Electroslag Refining on Removal of Iron Impurity and Alumina Inclusions from Aluminum. In *ICAA13 Pittsburgh, Proceedings of the 13th International Aluminium Alloys Conference on Aluminum Alloys (ICAA13), Pittsburgh, PA, USA, 3–7 June 2012*; Springer: Cham, Switzerland; Volume 13, pp. 207–212. [CrossRef]
20. Gao, J.W.; Shu, D.; Wang, J.; Sun, B.D. Effects of Na2B4O7 on the elimination of iron from aluminium melt. *Scr. Mater.* **2007**, *57*, 197–200. [CrossRef]
21. Flores, V.A.; Sukiennik, M.; Castillejos, E.A.H.; Acosta, G.F.A.; Escobedo, B.J.C. A kinetic study on the nucleation and growth of the Al8FeMnSi2 intermetallic compound for aluminum scrap purification. *Intermetallics* **1998**, *6*, 217–227. [CrossRef]
22. Khalifa, W.; Samuel, F.H.; Gruzleski, J.E.; Doty, H.W.; Valtierra, S. Nucleation of Fe-Intermetallic Phases in the Al-Si-Fe alloys. *Metall. Mater. Trans. A* **2005**, *36*, 1017–1032. [CrossRef]
23. Serak, J.; Vojtech, D.; Novak, P.; Sefl, V. Decrease of iron contents in AlSiCuMgFe alloys. In Proceedings of the 17th International Conference on Metallurgy and Materials (METAL 2008), Hradec nad Moravici, Czech Republic, 13–15 May 2008; pp. 1–6.
24. Cao, X.; Campbell, J. The nucleation of Fe-rich phases on oxide films in Al-11.5Si-0.4Mg cast alloys. *Metall. Mater. Trans. A* **2003**, *34*, 1409–1420. [CrossRef]

25. Cao, X.; Campbell, J. The solidification characteristics of Fe-rich intermetallics in Al-11.5Si-0.4Mg cast alloys. *Metall. Mater. Trans. A* **2004**, *35*, 1425–1435. [CrossRef]
26. Orozco-González, P.; Castro-Roman, M.; Maldonado-Ruiz, S.; Haro-Rodriguez, S.; Equihua-Guillen, F.; Muniz-Valdez, R.; Luna-Alvarez, S.; Montoya-Davila, M.; Hernandez-Rodriguez, A. Nucleation of Fe-Rich Intermetallic Phases on α-Al_2O_3 Oxide Films in Al-Si Alloys. *J. Miner. Mater. Charact. Eng.* **2015**, *3*, 15–25. [CrossRef]
27. Cao, X.; Saunders, N.; Campbell, J. Effect of iron and manganese contents on convection-free precipitation and sedimentation of primary-Al(FeMn)Si phase in liquid Al-11.5Si-0.4Mg alloy. *J. Mater. Sci.* **2004**, *39*, 2303–2314. [CrossRef]
28. Ferraro, S.; Fabrizi, A.; Timelli, G. Evolution of sludge particles in secondary die-cast aluminium alloys as function of Fe, Mn and Cr content. *Mater. Chem. Phys.* **2015**, *153*, 168–179. [CrossRef]
29. Wagner, R.; Seleznev, M.; Fischer, H.; Ditscherlein, R.; Becker, H.; Dietrich, B.G.; Keßler, A.; Leißner, T.; Wolf, G.; Leineweber, A.; et al. Impact of melt conditioning and filtration on iron-rich ß phase in AlSi9Cu3 and its fatigue life studied by µCT. *Mater. Charact.* **2021**, *174*, 111039. [CrossRef]
30. Timelli, G.; Capuzzi, S.; Fabrizi, A. Precipitation of primary Fe-rich compounds in secondary AlSi9Cu3(Fe) alloys. *J. Therm. Anal. Calorim.* **2016**, *123*, 249–262. [CrossRef]
31. Ji, S.; Gao, F.; Fan, Z. Thermodynamics Calculation of Extra Mn Addition in the Recycling of Al-Si-Cu Aluminium alloys. *Mater. Sci. Forum* **2016**, *877*, 33–38. [CrossRef]
32. Fan, Z.; Zuo, Y.B.; Jiang, B. A New Technology for Treating Liquid Metals with Intensive Melt Shearing. *Mater. Sci. Forum* **2011**, *690*, 141–144. [CrossRef]
33. Fan, Z.; Zuo, Y.B.; Jiang, B. Apparatus and Method for Liquid Metals Treatment. WO Patent 2012035357 A1, 22 March 2012.
34. Fan, Z.; Ji, S.; Stone, I. Purifying and Alloy Melt. WO Patent 2016146980 A1, 22 September 2016.
35. Tong, M.; Jagarlapudi, S.C.; Patel, J.B.; Stone, I.C.; Fan, Z.; Browne, D.J. Computational prediction of the refinement of oxide agglomerates in a physical conditioning process for molten aluminium alloy. In Proceedings of the IOP Conf. Series: Materials Science and Engineering, Hyogo, Japan, 21–26 June 2015; Volume 84, p. 012092. [CrossRef]
36. Dybalska, A.; Eskin, D.G.; Patel, J.B. Optimal Stator Design for Oxide Films Shearing Found by Physical Modelling. In *Materials Processing Fundamentals*; Springer: Cham, Switzerland, 2019; pp. 181–192. [CrossRef]
37. Li, H.T.; Ji, S.; Wang, Y.; Xia, M.; Fan, Z. Effect of intensive melt shearing on the formation of Fe-containing intermetallics in LM24 Al-alloy. In Proceedings of the IOP Conf. Series: Materials Science and Engineering, Kerkrade, The Netherlands, 7–10 June 2011; Volume 27, p. 012075. [CrossRef]
38. Chen, S.L.; Daniel, S.; Zhang, F.; Chang, Y.A.; Yan, X.Y.; Xie, F.Y.; Schmid-Fetzer, R.; Oatsed, W.A. The PANDAT software package and its applications. *Calphad* **2002**, *26*, 175–188. [CrossRef]
39. Pandat with Pan Al Database Version 2021. Available online: www.computherm.com (accessed on 6 September 2022).
40. Das, S.K. Designing Aluminium Alloys for a Recycling Friendly World. *Mater. Sci. Forum* **2006**, *519–521*, 1239–1244. [CrossRef]
41. Khalifa, W.; Samual, F.H.; Gruzleski, J.E. Iron intermetallic phases in the Al corner of the Al-Si-Fe system. *Metall. Mater. Trans. A* **2003**, *34*, 807–825. [CrossRef]
42. Basak, C.B.; Haribabu, H. Morphological changes and segregation of β-$Al9Fe_2Si_2$ phase: A perspective from better recyclability of cast Al-Si alloys. *Mater. Des.* **2016**, *108*, 277–288. [CrossRef]
43. Shabestari, S.G. The effect of iron and manganese on the formation of intermetallic compounds in aluminum–silicon alloys. *Mater. Sci. Eng. A* **2004**, *383*, 289–298. [CrossRef]
44. Yang, W.; Gao, F.; Ji, S. Formation and sedimentation of Fe-rich intermetallics in Al-Si-Cu-Fe alloy. *Trans. Nonferrous Met. Soc. China* **2015**, *25*, 1704–1714. [CrossRef]
45. Lazaro-Nebreda, J.; Patel, J.B.; Stone, I.; Scamans, G.M.; Fan, Z. De-Ironing of Aluminium Scrap by High Shear Melt Conditioning Technology. In Proceedings of the 6th Decennial International Conference on Solidification Processing (SP17), Windsor, UK, 25–28 July 2017; pp. 601–604.
46. Lazaro-Nebreda, J.; Patel, J.B.; Scamans, G.M.; Fan, Z. Multi-purpose high shear melt conditioning technology for effective melt quality and for recycling of Al-alloy scrap. In Proceedings of the 16th International Aluminium Alloys Conference on Aluminum Alloys (ICAA16), Montreal, QC, Canada, 17–21 June 2018; p. 401623.
47. Scamans, G.M.; Li, H.T.; Lazaro-Nebreda, J.; Patel, J.B.; Stone, I.; Wang, Y.; Yang, X.; Fan, Z. Chapter 8—Advanced Casting Technologies Using High Shear Melt Conditioning. In *Fundamentals of Aluminium Metallurgy*; Woodhead Publishing: Cambridge, UK, 2018; pp. 249–277. [CrossRef]
48. Lazaro-Nebreda, J.; Patel, J.B.; Chang, I.T.H.; Stone, I.C.; Fan, Z. Solidification processing of scrap Al-alloys containing high levels of Fe. In Proceedings of the IOP Conference Series: Materials Science and Engineering, Salzburg, Austria, 17–21 June 2019; Volume 529, p. 012059. [CrossRef]
49. Al-Helal, K.; Lazaro-Nebreda, J.; Patel, J.B.; Scamans, G.M. High-Shear De-Gassing and De-Ironing of an Aluminum Casting Alloy Made Directly from Aluminum End-of-Life Vehicle Scrap. *Recycling* **2021**, *6*, 66. [CrossRef]
50. Tong, M.; Patel, J.B.; Stone, I.; Fan, Z.; Browne, D.J. Identification of key liquid metal flow features in the physical conditioning of molten aluminium alloy with high shear processing. *Comput. Mater. Sci.* **2017**, *131*, 35–43. [CrossRef]
51. Tong, M.; Patel, J.B.; Stone, I.; Fan, Z.; Browne, D.J. The Scale-Up of High Shear Processing for the Purification of Recycled Molten Scrap Aluminium Alloy: Key Features of Fluid Flow. In *Light Metals*; Springer: Cham, Switzerland, 2017; pp. 1123–1129. [CrossRef]

52. Dybalska, A.; Eskin, D.G.; Patel, J.B. Validation of the Physical Simulations of a Stirred Molten Metal Using Particle Image Velocimetry Data. *JOM* **2018**, *70*, 1256–1260. [CrossRef]
53. Lazaro-Nebreda, J.; Patel, J.B.; Fan, Z. Improved degassing efficiency and mechanical properties of A356 aluminium alloy castings by high shear melt conditioning (HSMC) technology. *J. Mater. Process. Technol.* **2021**, *294*, 117146. [CrossRef]
54. Dybalska, A.; Eskin, D.; Patel, J.B. Evaluation of Shearing Time Sufficient for Effective Liquid Metal Processing. *JOM* **2017**, *69*, 720–724. [CrossRef]
55. Hakansson, A. Rotor-Stator mixers: From batch to continuous mode of operation-A review. *Processes* **2018**, *6*, 32. [CrossRef]
56. Lebon, G.S.B.; Lazaro-Nebreda, J.; Patel, J.B.; Fan, Z. Numerical Assessment of In-Line Rotor–Stator Mixers in High-Shear Melt Conditioning (HSMC) Technology. *JOM* **2020**, *72*, 4092–4100. [CrossRef]
57. Cinkilic, E.; Ridgeway, C.D.; Yan, X.; Luo, A.A. A Formation Map of Iron-Containing Intermetallic Phases in Recycled Cast Aluminium Alloys. *Metall. Mater. Trans. A* **2019**, *50*, 5945–5956. [CrossRef]
58. Song, D.; Zhao, Y.; Jia, Y.; Li, R.; Zhou, N.; Zheng, K.; Fu, Y.; Zhang, W. Study of the evolution mechanisms of Fe-rich phases in Al-Si-Fe alloys with Mn modification using synchrotron X-ray imaging. *J. Alloys Compd.* **2022**, *915*, 165378. [CrossRef]
59. Song, D.; Zhao, Y.; Wang, Z.; Jia, Y.; Huang, H.; Zhang, D.; Zhang, W. Effect of Mn/Fe ratio on Fe removal efficiency and tensile ductility of and Al-7.0Si-2.4Fe alloy. *J. Mater. Res.* **2021**, *36*, 1357–1366. [CrossRef]
60. Cinkilic, E.; Moodispaw, M.; Zhang, J.; Miao, J.; Luo, A.A. A New Recycled Al-Si-Mg Alloy for Sustainable Structural Die Casting Applications. *Metall. Mater. Trans. A* **2022**, *53*, 2861–2873. [CrossRef]
61. Gnatko, M.; Li, C.; Arnold, A.; Friedrich, B. Purification of Aluminium Cast Alloy Melts through Precipitation of Fe-Containing Intermetallic Compounds. *Metals* **2018**, *8*, 796. [CrossRef]
62. Que, Z.; Wang, Y.; Fan, Z. Formation of the Fe-containing intermetallic compounds during solidification of Al-5Mg-2Si-0.7Mn-1.1Fe alloy. *Mater. Metall. Trans. A* **2018**, *49*, 2173–2181. [CrossRef]
63. Men, H.; Jiang, B.; Fan, Z. Mechanisms of grain refinement by intensive shearing of AZ91 alloy melt. *Acta Mater.* **2010**, *58*, 6526–6534. [CrossRef]
64. Liu, Y.; Huang, G.; Sun, Y.; Zhang, L.; Huang, Z.; Wang, J.; Liu, C. Effect of Mn and Fe on the formation of Fe-rich intermetallics in Al-5Mg-Mn alloys solidified under rapid cooling. *Materials* **2016**, *9*, 88. [CrossRef]
65. Gyarmati, G.; Bubonyi, T.; Fegyverneki, G.; Tokar, M.; Mende, T. Interactions of primary intermetallic compound particles and double oxide films in liquid aluminium alloys. *Intermetallics* **2022**, *149*, 107681. [CrossRef]
66. Feng, S.; Liotti, E.; Lui, A.; Wilson, M.D.; Grant, P. Nucleation bursts of primary intermetallic crystals in a liquid Al alloy studied using in situ synchrotron X-ray radiography. *Acta Materialia* **2021**, *221*, 117389. [CrossRef]
67. Bjunrenstedt, A.; Casari, D.; Seifeddine, S.; Mathiesen, R.H.; Dahle, A.K. In-situ study of morphology and growth of primary α-Al(FeMnCr)Si intermetallics in an Al-Si alloy. *Acta Mater.* **2017**, *130*, 1–9. [CrossRef]
68. Gaustad, G.; Olivetti, E.; Kirchain, R. Improving aluminum recycling: A survey of sorting and impurity removal technologies. *Resour. Conserv. Recycl.* **2012**, *58*, 79–87. [CrossRef]
69. Peng, L.; Zeng, G.; Su, T.U.; Yasuda, H.; Nogita, K.; Gourlay, C.M. Al8Mn5 Particle Settling and Interactions with Oxide Films in Liquid AZ91 Manesium Alloys. *JOM* **2019**, *71*, 2235–2244. [CrossRef]
70. Rogler, J.P.; Heaslip, L.J.; Mehrvar, M. Inclusion removal in a tundish by gas bubbling. *Can. Metall. Q.* **2004**, *43*, 407–415. [CrossRef]